molecules

MDPI

Article

Small Peptides Able to Suppress Prostaglandin E_2 Generation in Renal Mesangial Cells

Sofia Vasilakaki [1], Oleksandr Pastukhov [2], Thomas Mavromoustakos [1], Andrea Huwiler [2] and George Kokotos [1,*]

[1] Laboratory of Organic Chemistry, Department of Chemistry, National and Kapodistrian University of Athens, Panepistimiopolis, Athens 15771, Greece; svasilak@chem.uoa.gr (S.V.); tmavrom@chem.uoa.gr (T.M.)

[2] Institute of Pharmacology, University of Bern, Bern 3010, Switzerland; oleksandr.pastukhov@kispi.uzh.ch (O.P.); huwiler@pki.unibe.ch (A.H.)

* Correspondence: gkokotos@chem.uoa.gr; Tel.: +30-210-727-4462

Received: 22 December 2017; Accepted: 10 January 2018; Published: 13 January 2018

Abstract: Peptide drug discovery may play a key role in the identification of novel medicinal agents. Here, we present the development of novel small peptides able to suppress the production of PGE_2 in mesangial cells. The new compounds were generated by structural alterations applied on GK115, a novel inhibitor of secreted phospholipase A_2, which has been previously shown to reduce PGE_2 synthesis in rat renal mesangial cells. Among the synthesized compounds, the tripeptide derivative **11** exhibited a nice dose-dependent suppression of PGE_2 production, similar to that observed for GK115.

Keywords: inhibitors; mesangial cells; peptides; prostaglandin E_2; secreted phospholipase A_2

1. Introduction

Prostaglandin E_2 (PGE_2) is one of the most important lipid mediators [1] playing a pivotal role in inflammatory diseases [2] including glomerulonephritis. Glomerulonephritis is initiated by the invasion of activated immune cells into the renal glomerulus and the release of pro-inflammatory cytokines such as TNFα and interleukin (IL) 1β to activate the local resident mesangial cells [3,4]. This activation includes three main responses, i.e., increased proliferation, increased matrix production, and increased inflammatory mediator production, which are all hallmarks of glomerulonephritis, finally resulting in glomerulosclerosis and renal failure [4]. Due to this central involvement of mesangial cells in the pathogenesis of chronic inflammatory kidney diseases, they serve as a useful cellular model system to test for new therapeutic compounds to treat such diseases.

The biosynthesis of PGE_2 is initiated by the action of phospholipases A_2 (PLA_2), which cleave the *sn*-2 ester bond of membrane glycerophospholipids to release arachidonic acid [5,6]. Then, arachidonic acid is converted to PGH_2 and the terminal step of PGE_2 generation is catalyzed by microsomal prostaglandin synthase-1 [7]. Four types of PLA_2 [6] are expressed at mesangial cells: cytosolic ($cPLA_2$) GIVA, calcium-independent ($iPLA_2$) GVIA and secreted ($sPLA_2$) GIIA and GV [8–10]. It has been demonstrated that the progression of glomerular inflammatory processes is a result of a network of interactions between different PLA_2s [9] and a cross-talk between $cPLA_2$ and $sPLA_2$ has been reported in hydrogen peroxide-induced arachidonic acid release in murine mesangial cells [11]. In addition, $sPLA_2$ GIIA seems to have multiple roles in mesangial cells inducing the production of pro-inflammatory mediators [12].

We have recently demonstrated that inhibitors of $sPLA_2$ suppress the release of PGE_2 formation in renal mesangial cells [13]. Four such inhibitors presented an interesting effect on the suppression of PGE_2 release and their structures are shown in Figure 1. Inhibitors **1** (GK115) [14] and **2** [15] are amides based on the non-natural amino acids γ-norleucine and γ-tyrosine, respectively, while inhibitors **3**

(GK126) [16] and **4** (GK241) [17] are 2-oxoamides based on the natural amino acids leucine and valine, respectively. As depicted in Figure 1, all of them are characterized by high lipophilicity (ClogP value higher than 5), an unfavorable property according to Lipinski's rule of 5 [18]. The ClogP values of the inhibitors were calculated using ChemOffice Ultra 11.00.

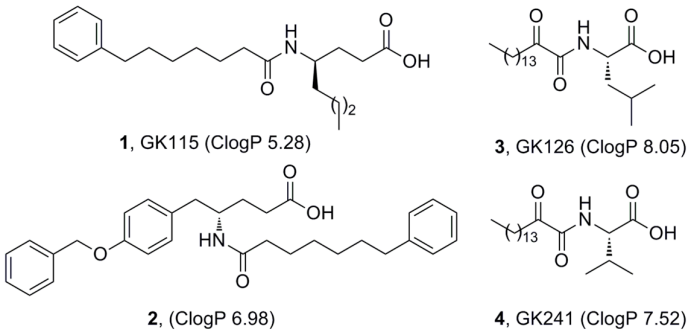

Figure 1. Inhibitors of secreted PLA_2 able to suppress the formation of PGE_2 in mesangial cells.

Over the last years, peptide drug discovery has experienced a revival of interest, as the pharmaceutical industry has come to appreciate the role that peptides may play in addressing unmet medical needs and how peptides can be an excellent complement to small molecule medicinal agents [19]. In an effort to identify novel compounds able to suppress the formation of PGE_2, in the current work we explored the possibility of small conjugated peptides to inhibit the release of PGE_2 at a cellular level. Herein, we report the structure-based design and synthesis of several small peptides derivatives (Figure 2), whose structures are inspired by the structures of $sPLA_2$ inhibitors described above, and the evaluation of their ability to suppress PGE_2 formation.

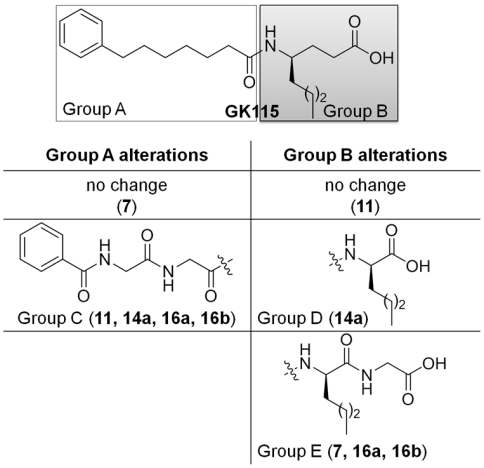

Figure 2. The design of new inhibitors was based on alterations of Groups A and B of GK115 structure. The table describes the alterations of Groups A and B and the corresponded generated compounds in brackets.

2. Results

2.1. Synthesis

Inspired by the structure of inhibitor GK115 and considering it as a lead compound, we designed derivatives replacing the γ-norleucine residue by α-norleucine or a norleucine based dipeptide. In addition, and in an effort to decrease the lipophilicity of the compounds, we replaced the acyl chain

of GK115 (Group A, Figure 2) by a chain based on the benzoyl derivative of the peptide glycyl-glycine (Group C, Figure 2).

Compound **7** was synthesized by coupling of 7-phenyl-heptanoic acid **5** with the dipeptide norleucyl-glycine using 1-(3-dimethylaminopropyl)-3-ethyl carbodiimide (WSCI) as a condensing agent in the presence of 1-hydroxybenzotriazole (HOBt), followed by alkaline hydrolysis (Scheme 1).

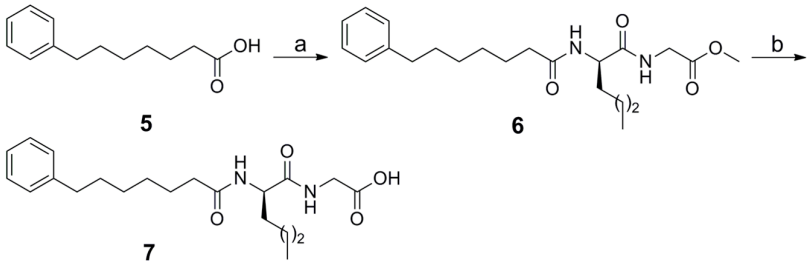

Scheme 1. *Reagents and conditions*: a. H-Nle-Gly-OMe, WSCI·HCl, HOBt, Et_3N, CH_2Cl_2; b. 1 N aq NaOH, MeOH.

Compound **11**, where the acyl chain of GK115 was replaced by the benzoyl derivative of the dipeptide glycyl-glycine, was synthesized by coupling of benzoyl-glycyl-glycine **8** with methyl γ-norleucinate **9**, as depicted in Scheme 2.

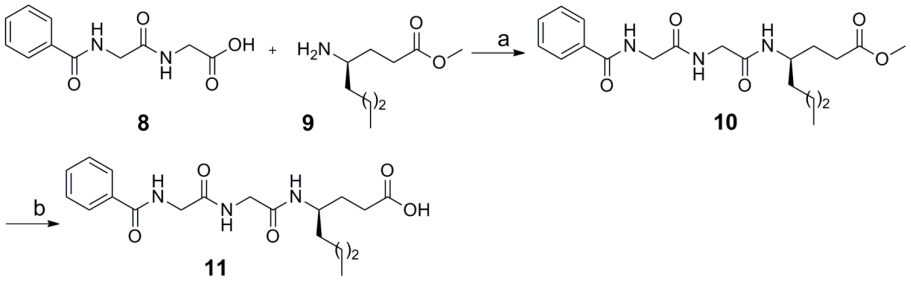

Scheme 2. *Reagents and conditions*: a. WSCI·HCl, HOBt, Et_3N, CH_2Cl_2; b. 1 N aq NaOH, MeOH.

To synthesize derivatives based on either α-norleucine or the dipeptide norleucyl-glycine, benzoyl-glycine **12** was coupled with methyl norleucyl-glycinate (Scheme 3). After alkaline hydrolysis, compounds **14a** and **14b** based on (*R*)- and (*S*)-norleucine, respectively, were obtained. Coupling of **14a** with *tert*-butyl glycinate led to compound **16a** after acidic hydrolysis.

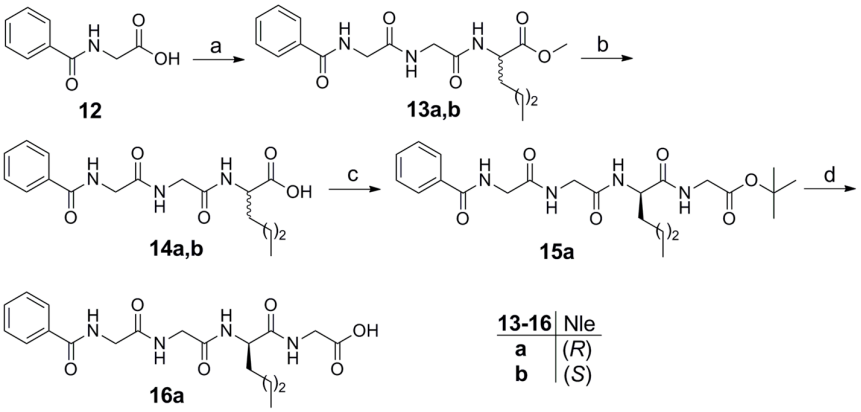

Scheme 3. *Reagents and conditions*: a. H-Gly-Nle-OMe, WSCI·HCl, HOBt, Et_3N, CH_2Cl_2; b. 1 N aq NaOH, MeOH; c. H-Gly-O*t*Bu, WSCI·HCl, HOBt, Et_3N, CH_2Cl_2; d. CF_3COOH, CH_2Cl_2.

2.2. Suppression of PGE_2 Release in Mesangial Cells

Cultures of rat renal mesangial cells were stimulated for 24 h with IL-1β plus forskolin (Fk) to trigger a huge increase of PGE_2 synthesis, as previously described [20]. Cells were treated in the absence or presence of three different concentrations (1 μM, 3 μM and 10 μM) of the various synthetic compounds. Supernatants were collected and subjected to PGE_2-ELISA to quantify PGE_2 released from the cells.

The results of the suppression of PGE_2 release in mesangial cells caused by the new peptides derivatives are shown in Figure 3. In the absence of IL-1β plus Fk, none of the compounds, tested at the highest concentration of 10 μM, changed the basal PGE_2 synthesis significantly (data not shown).

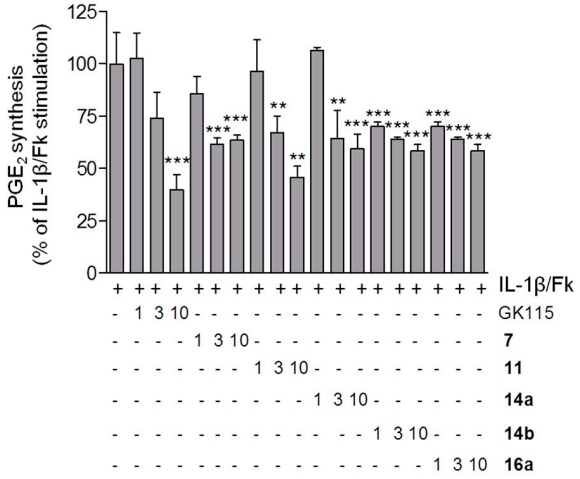

Figure 3. Effect of compounds **7**, **11**, **14a**, **14b** and **16a** on IL-1β/Fk-stimulated PGE_2 formation in mesangial cells. Data are presented as % of maximal IL-1β/Fk stimulation and are means ± S.D. (n = 3). ** $p < 0.01$, *** $p < 0.001$ considered statistical significant when compared to the IL-1β/Fk samples. Basal PGE_2 concentration was at 7.9 ± 5.3 pg/100 μL supernatant; the maximal IL-1β/Fk-stimulated PGE_2 concentration was at 685 ± 81 pg/100 μL supernatant.

Most of the peptides derivatives tested were able to reduce the release of PGE_2. The replacement of γ-norleucine by the dipeptide Nle-Gly (compound **7**) did not cause any remarkable difference in activity. The tripeptide derivative **11** exhibited a nice dose-dependent curve similar to that observed for GK115. The replacement of the hydrocarbon acyl chain of GK115 by the dipeptide glycyl-glycine chain resulted in a considerable decrease of the lipophilicity, dropping the ClogP value from 5.28 to 1.73. It should be noticed that this derivative seems efficiently protected by the action of both aminopeptidases and carboxypeptidases. Peptides based on γ-amino acids are resistant to carboxypeptidases [21], while the benzoyl protecting group offers resistance to aminopeptidases. Tripeptides **14a** and **14b** and tetrapeptide **16a** derivatives exhibited similar ability to suppress PGE_2 formation irrespectively of either the stereochemistry of norleucine (*R* in **14a** and *S* in **14b**) or the size of the peptide (tripeptide versus tetrapeptide). Peptide incorporation of segments in **13a**, **14b** and **16a** resulted in reduced lipophilicities with ClogP values of 1.51, 1.51 and 0.94, respectively. These results confirm our hypothesis that we could improve compounds' lipophilicity, while preserve their potency to suppress PGE_2 release.

2.3. Docking Studies

Since we have shown that inhibition of $sPLA_2$ is a possible path via which our $sPLA_2$ inhibitors (GK115, GK126 and GK241) evoke the suppression of PGE_2 release [13], we performed docking calculations for the binding pose prediction of compounds GK115 and **11** in the active site of the enzyme.

Sybyl 8.0 [22] by TRIPOS was used for the design and the energy minimization of the structures. The carboxyl group was considered deprotonated and the Powell algorithm was used for the energy minimization. The crystal structure of $sPLA_2$ GIIA was retrieved from the Brookhaven Protein Databank (code: 1KQU) and used for the docking calculations. The protein's missing loops were added with the Prime module of Schrödinger Suite [23]. The molecules were placed in the active site of the enzyme manually in Chimera [24] and docked in AutoDock Vina [25].

By visual inspection of the docking results, docking poses which reproduced the known interactions between the co-crystallized ligands and the enzyme, were chosen and subjected to molecular dynamics (MD) simulations with AMBER14 [26], following a standard procedure [17]. MD simulations (100 ns) were run and the top cluster of each simulation is shown in Figures 4 and 5. For the clustering, the hieragglo algorithm was used and the *averagelinkage* option in *cpptraj* [27] was defined using the Leu2, Phe5, His6, Ile9, Ala17-Gly32, Cys44, His47, Asp48, Lys62, Asp91 and Phe98 amino acids.

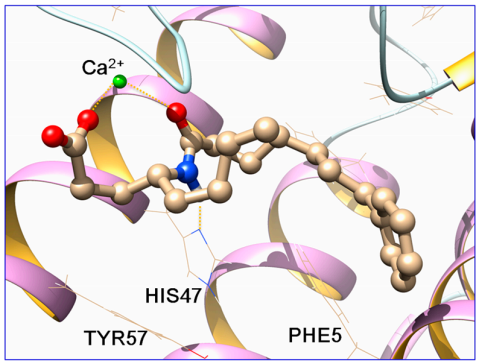

Figure 4. Binding pose prediction of GK115 in the active site of $sPLA_2$ GIIA (red: oxygen atoms, blue: nitrogen atoms, green: calcium atom).

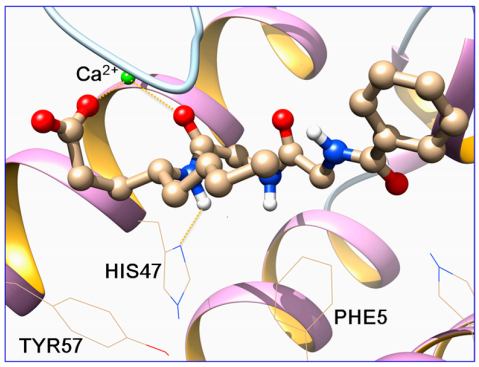

Figure 5. Binding pose prediction of **11** in the active site of $sPLA_2$ GIIA (red: oxygen atoms, blue: nitrogen atoms, green: calcium atom).

The carboxyl group of both molecules and the carbonyl group of the Nle-Gly peptide bond of **11** and the amide group of GK115 chelate the Ca^{2+} ion throughout the simulation time. Additionally, a hydrogen bond is formed between His47 and the -NH group of the peptide bond of **11** and the amide group of GK115, respectively. These interactions are present in the crystallized structures of $sPLA_2$ GIIA with the native ligands [15]. Both inhibitors adopt similar conformation in the active site and they preserve it, with small fluctuations, during the MD time (Figure 6).

This further contributes to the persistence of the interactions between the molecules and the residues of the active site. MM-PBSA [28] method was used for the estimation of the energetic terms of both systems. The ΔH value for inhibitor GK115 is −47.16 kcal/mol with a standard deviation error (SDE) 5.16 kcal/mol and for compound **11** is −38.22 kcal/mol with SDE of 6.26 kcal/mol. Since GK115

is a potent inhibitor of $sPLA_2$ GIIA, both the key interactions and the ΔH values calculated by the MD trajectories are a good indicator of a possible inhibition of $sPLA_2$ GIIA by **11** and biological assays will be performed in a future study to investigate this possibility.

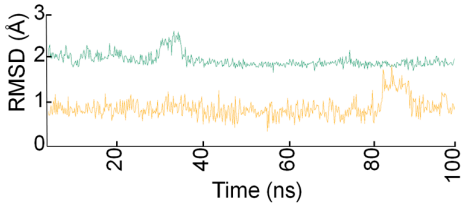

Figure 6. Root-mean-square deviation (RMSD) values of inhibitors **11** (green) and GK115 (orange) in the active site of $sPLA_2$ GIIA during the MD simulation time.

3. Discussion

Our studies led to the identification of a number of small peptides derivatives that present a significant suppression of PGE_2 release in renal mesangial cells. Among them, benzoyl-glycyl-glycyl-γ-(*R*)-norleucine (**11**) showed an interesting effect on the suppression of PGE_2 formation. This tripeptide derivative has a significant lower lipophilicity in comparison to the lead compound GK115 without loss of the ability to suppress PGE_2 release at a cellular level. Thus, new agents that can serve as leads to reduce pathological PGE_2 production, as seen in chronic inflammatory kidney diseases such as glomerulonephritis, have been identified.

4. Materials and Methods

4.1. Chemistry

Merck Silica Gel 60 (70–230 or 230–400 mesh) (Merck Co., Darmstadt, Germany) was used for the chromatographic purification of products and Silica Gel 60 F254 (Merck Co., Darmstadt, Germany) aluminum plates for the thin-layer chromatography (TLC). UV light and/or phosphomolybdic acid in EtOH was employed for visualizing shpots. A Büchi 530 apparatus (Buchi, Flawil, Switzerland) was used to estimate melting points and they were uncorrected. ^1H and ^{13}C–NMR spectra were recorded on Varian Mercury (Varian Inc., Palo Alto, CA, USA) at 200 MHz and 50 MHz respectively. Samples were diluted in $CDCl_3$, CD_3OD, DMSO or D_2O. Chemical shifts are given in ppm, and coupling constants (*J*) in Hz. Peak multiplicities are typified as: s, singlet, d, doublet, t, triplet and m, multiplet. Electron spray ionization (ESI) mass spectra were recorded on a Finnigan, Surveyor MSQ Plus spectrometer (Thermo Finnigan, Ringoes, NJ, USA). Specific rotations of the compounds were measured at 25 °C on a Perkin-Elmer 343 polarimeter (PerkinElmer Inc., Shelton, CT, USA) using a 10 cm cell. Dichloromethane was dried by standard procedures and stored over molecular sieves. No further purification of other solvents and chemicals needed as they were reagent grade. HRMS spectra were recorded on a Bruker Maxis Impact QTOF Spectrometer (Bruker Daltonics, Billerica, MA, USA).

4.1.1. Coupling Method

To a stirred solution of hydrochloride amino component (1.0 mmol) in CH_2Cl_2 (10 mL), Et_3N (0.3 mL, 2.2 mmol) and subsequently WSCI·HCl (0.21 g, 1.1 mmol) and HOBt (0.14 g, 1.0 mmol) were added at 0 °C. The acid component (1.0 mmol) was added and the reaction mixture was stirred for 1 h at 0 °C and then overnight at room temperature. After the completion of the reaction, the solvent was evaporated under reduced pressure and EtOAc (20 mL) was added. The organic layer was washed consecutively with brine, 1 N aqueous HCl, brine, 5% $NaHCO_3$, and brine, dried over Na_2SO_4 and evaporated under reduced pressure. The residue was purified by column chromatography [EtOAc/petroleum ether (bp 40–60 °C), 2:8].

(R)-Methyl 2-(2-(7-phenylheptanamido)hexanamido)acetate (**6**). Yield 77%; Colorless oil; $[\alpha]_D^{20}$ + 33.0 (*c* 1.00, CH_3OH); ^{1}H–NMR ($CDCl_3$, 200 MHz): δ 7.72 (t, *J* = 5.5 Hz, 1H, NH), 7.33–7.07 (m, 5H, arom), 6.91 (d, *J* = 8.3 Hz, 1H, NH), 4.63 (dt, *J* = 7.5 Hz, 1H, NHC*H*), 4.19–3.81 (m, 2H, NHCH_2), 3.68 (s, 3H, $COOCH_3$), 2.57 (t, *J* = 7.6 Hz, 2H, CH_2), 2.19 (t, *J* = 7.4 Hz, 2H, NHCOCH_2), 1.92–1.45 (m, 6H, CH_2), 1.44–1.16 (m, 8H, CH_2), 0.87 (t, *J* = 6.7 Hz, 3H, CH_3); ^{13}C–NMR ($CDCl_3$, 50 MHz): δ 173.3, 172.8, 169.8, 142.4, 128.5, 128.0, 125.4, 52.6, 52.0, 40.9, 36.1, 35.7, 32.2, 31.6, 28.9, 28.8, 27.4, 25.4, 22.3, 13.8; MS (ESI) *m*/*z* (%): 391.14 (92) $[M + H]^+$; Anal. Calcd for $C_{22}H_{34}N_2O_4$: C, 67.66; H, 8.78; N, 7.17. Found: C, 67.49; H, 8.97; N, 7.03.

(R)-Methyl 4-(2-(2-benzamidoacetamido)acetamido)octanoate (**10**). Yield 62%; Yellow oil; $[\alpha]_D^{20}$ + 1.5 (*c* 1.00, $CHCl_3$); ^{1}H–NMR ($CDCl_3$, 200 MHz): δ 8.19–8.02 (m, 1H, N*H*), 7.87–7.67 (m, 3H, NH & arom), 7.51–7.24 (m, 3H, NH & arom), 7.03–6.86 (m, 1H, arom), 4.03 (d, *J* = 4.5 Hz, 2H, NHCH_2), 3.85 (d, *J* = 5.0 Hz, 2H, NHCH_2), 3.75–3.69 (m, 1H, NHC*H*), 3.53 (s, 3H, $COOCH_3$), 2.26 (t, *J* = 7.3 Hz, 2H, CH_2COO), 1.92–1.52 (m, 2H, NHCHCH_2), 1.48–1.03 (m, 6H, CH_2), 0.87–0.65 (m, 3H, CH_3); ^{13}C–NMR ($CDCl_3$, 50 MHz): δ 174.1, 170.1, 168.8, 168.3, 132.9, 131.8, 128.4, 127.2, 51.5, 49.0, 43.9, 43.0, 34.5, 30.5, 29.7, 27.9, 22.4, 13.8; MS (ESI) *m*/*z* (%): 392.14 (90) $[M + H]^+$; Anal. Calcd for $C_{20}H_{29}N_3O_5$: C, 61.36; H, 7.47; N, 10.73. Found: C, 61.15; H, 7.74; N, 10.54.

(R)-Methyl 2-(2-(2-benzamidoacetamido)acetamido)hexanoate (**13a**). Yield 53%; White solid; mp 140–142 °C; $[\alpha]_D^{20}$ + 18.6 (*c* 1.02, $CHCl_3$); ^{1}H–NMR ($CDCl_3$, 200 MHz): δ 7.95–7.66 (m, 4H, NH & arom), 7.52–7.27 (m, 4H, arom), 4.45 (dt, *J* = 7.5 Hz, 1H, NHC*H*), 4.10 (d, *J* = 5.1 Hz, 2H, NHCH_2), 4.06–3.82 (m, 2H, NHCH_2), 3.63 (s, 3H, $COOCH_3$), 1.86–1.49 (m, 2H, NHCHCH_2), 1.34–1.09 (m, 4H, CH_2), 0.80 (t, *J* = 6.6 Hz, 3H, CH_3); ^{13}C–NMR ($CDCl_3$, 50 MHz): δ 173.0, 170.2, 169.2, 168.1, 133.2, 131.7, 128.4, 127.2, 52.4, 52.2, 43.7, 42.8, 31.4, 27.4, 22.1, 13.7; MS (ESI) *m*/*z* (%): 364.09 (90) $[M + H]^+$; Anal. Calcd for $C_{18}H_{25}N_3O_5$: C, 59.49; H, 6.93; N, 11.56. Found: C, 59.40; H, 7.03; N, 11.47.

(S)-Methyl 2-(2-(2-benzamidoacetamido)acetamido)hexanoate (**13b**). Yield 68%; White solid; mp 139–141 °C; $[\alpha]_D^{20}$ − 18.0 (*c* 1.00, $CHCl_3$); ^{1}H–NMR ($CDCl_3$, 200 MHz): δ 8.04 (t, *J* = 4.9 Hz, 1H, NH), 7.88 (t, *J* = 5.1 Hz, 1H, NH), 7.83–7.69 (m, 2H, NH & arom), 7.62–7.46 (m, 1H, arom), 7.45–7.19 (m, 3H, arom), 4.40 (dt, *J* = 7.6 Hz, 1H, NHC*H*), 4.06 (d, *J* = 4.7 Hz, 2H, NHCH_2), 4.00–3.80 (m, 2H, NHCH_2), 3.59 (s, 3H, $COOCH_3$), 1.86–1.47 (m, 2H, NHCHCH_2), 1.32–1.05 (m, 4H, CH_2), 0.77 (t, *J* = 6.7 Hz, 3H, CH_3); ^{13}C–NMR ($CDCl_3$, 50 MHz): δ 173.0, 170.2, 169.2, 168.1, 133.1, 131.6, 128.2, 127.2, 52.3, 52.0, 43.6, 42.7, 31.3, 27.4, 22.0, 13.6; MS (ESI) *m*/*z* (%): 364.04 (90) $[M + H]^+$; Anal. Calcd for $C_{18}H_{25}N_3O_5$: C, 59.49; H, 6.93; N, 11.56. Found: C, 59.20; H, 7.15; N, 11.35.

(R)-tert-Butyl 9-butyl-1,4,7,10-tetraoxo-1-phenyl-2,5,8,11-tetraazatridecan-13-oate (**15a**). Yield 92%; White solid; mp 177–178 °C; $[\alpha]_D^{20}$ + 11.0 (*c* 1.00, CH_3OH); ^{1}H–NMR ($CDCl_3$, 200 MHz): δ 8.25–8.07 (m, 1H, NH), 8.05–7.94 (m, 1H, NH), 7.93–7.76 (m, 3H, NH & arom), 7.75–7.58 (m, 1H, arom), 7.55–7.29 (m, 3H, arom), 4.96–4.74 (m, 1H, NHC*H*), 4.43–4.25 (m, 2H, NHCH_2), 4.22–4.03 (m, 2H, NHCH_2), 4.01–3.71 (m, 2H, NHCH_2), 1.94–1.49 (m, 2H, CH_2), 1.40 (s, 9H, CH_3), 1.33–1.10 (m, 4H, CH_2), 0.81 (t, *J* = 6.7 Hz, 3H, CH_3); ^{13}C–NMR ($CDCl_3$, 50 MHz): δ 172.2, 169.6, 168.7, 168.5, 167.9, 133.5, 131.6, 128.3, 127.4, 81.9, 53.0, 43.5, 41.9, 33.1, 27.9, 27.5, 25.9, 22.4, 13.9; MS (ESI) *m*/*z* (%): 463.22 (90) $[M + H]^+$; Anal. Calcd for $C_{23}H_{34}N_4O_6$: C, 59.72; H, 7.41; N, 12.11. Found: C, 59.44; H, 7.70; N, 11.93.

4.1.2. Saponification of Methyl Esters

To a stirred solution of a methyl ester (1.0 mmol) in water, 1 N aqueous NaOH (1 mL, 1.0 mmol) was added and the mixture was left under stirring overnight at room temperature. After the completion of the reaction, the mixture was washed with EtOAc (3 × 10 mL), acidified with 1 N aqueous HCl to pH 1 and extracted with EtOAc (3 × 10 mL). The combined organic layers were washed with brine, dried over Na_2SO_4 and evaporated under reduced pressure.

(R)-2-(2-(7-Phenylheptanamido)hexanamido)acetic acid (**7**). Yield 83%; White oil; $[\alpha]_D^{20}$ + 15.0 (*c* 1.00, CH_3OH); ^{1}H–NMR ($CDCl_3$, 200 MHz): δ 9.67 (br s, 1H, COOH), 7.72–7.45 (m, 2H, NH), 7.36–6.99 (m, 5H, arom), 4.76–4.51 (m, 1H, NHC*H*), 4.13–3.86 (br s, 2H, NHCH_2), 2.69–2.39 (m, 2H, CH_2), 2.31–2.05 (m, 2H, NHCOCH_2), 1.92–1.45 (m, 6H, CH_2), 1.41–1.05 (m, 8H, CH_2), 0.96–0.69 (m, 3H, CH_3); ^{13}C–NMR

($CDCl_3$, 50 MHz): δ 174.3, 172.9, 172.0, 142.5, 128.2, 128.1, 125.5, 52.8, 41.2, 36.1, 35.7, 32.1, 31.2, 28.9, 28.9, 27.4, 25.5, 22.2, 13.8; HRMS (ESI) calcd for $C_{21}H_{33}N_2O_4$ $[M + H]^+$: 377.2435. Found: 377.2438; Anal. Calcd for $C_{21}H_{32}N_2O_4$: C, 66.99; H, 8.57; N, 7.44. Found: C, 66.72; H, 8.86; N, 7.27.

(R)-4-(2-(2-Benzamidoacetamido)acetamido)octanoic acid (**11**). Yield 88%; White solid; mp 202–204 °C; $[\alpha]_D^{20}$ + 4.0 (c 1.00, CH_3OH); ^{1}H–NMR (D_2O, 200 MHz): δ 7.89–7.70 (m, 2H, arom), 7.68–7.41 (m, 3H, arom), 4.07 (s, 2H, NHCH_2), 3.88 (s, 2H, NHCH_2), 3.82–3.64 (m, 1H, NHC*H*), 2.10 (t, *J* = 6.7 Hz, 2H, CH_2COOH), 1.93–1.06 (m, 8H, CH_2), 0.89–0.66 (m, 3H, CH_3); ^{13}C–NMR (D_2O, 50 MHz): δ 182.9, 172.4, 171.4, 170.9, 132.7, 132.5, 128.9, 127.4, 50.0, 34.2, 33.6, 31.2, 27.5, 21.9, 13.4; HRMS (ESI) calcd for $C_{19}H_{28}N_3O_5$ $[M + H]^+$: 378.2023. Found: 378.2025; Anal. Calcd for $C_{19}H_{27}N_3O_5$: C, 60.46; H, 7.21; N, 11.13. Found: C, 60.25; H, 7.42; N, 11.01.

(R)-2-(2-(2-Benzamidoacetamido)acetamido)hexanoic acid (**14a**). Yield 93%; White solid; mp 213–215 °C; $[\alpha]_D^{20}$ + 8.6 (*c* 1.00, CH_3OH); ^{1}H–NMR (DMSO, 200 MHz): δ 8.84 (t, *J* = 5.6 Hz, 1H, NH), 8.19 (t, *J* = 5.5 Hz, 1H, NH), 8.05–7.70 (m, 3H, NH & arom), 7.58–7.24 (m, 3H, arom), 4.22–4.02 (m, 1H, NHC*H*), 3.85 (d, *J* = 5.6 Hz, 2H, NHCH_2), 3.72 (d, *J* = 5.6 Hz, 2H, NHCH_2), 1.76–1.43 (m, 2H, CH_2), 1.35–1.01 (m, 4H, CH_2), 0.79 (t, *J* = 6.5 Hz, 3H, CH_3); ^{13}C–NMR (DMSO, 50 MHz): δ 173.6, 169.3, 168.8, 166.7, 133.9, 131.5, 128.3, 127.4, 51.8, 42.9, 41.8 30.8, 27.5, 21.8, 13.8; HRMS (ESI) calcd for $C_{17}H_{24}N_3O_5$ $[M + H]^+$: 350.1710. Found: 350.1711; Anal. Calcd for $C_{17}H_{23}N_3O_5$: C, 58.44; H, 6.64; N, 12.03. Found: C, 58.22; H, 6.86; N, 11.87.

(S)-2-(2-(2-Benzamidoacetamido)acetamido)hexanoic acid (**14b**). Yield 91%; White solid; mp 192–201 °C; $[\alpha]_D^{20}$ − 8.1 (*c* 1.08, CH_3OH); ^{1}H–NMR ($CDCl_3$ and drops CD_3OD, 200 MHz): δ 7.82–7.58 (m, 1H, arom), 7.53–7.14 (m, 4H, arom), 4.38–4.21 (m, 1H, NHC*H*), 4.05 (s, 2H, NHCH_2), 3.96 (s, 2H, NHCH_2), 1.87–1.43 (m, 2H, CH_2), 1.34–1.09 (m, 4H, CH_2), 0.75 (t, *J* = 6.5 Hz, 3H, CH_3); ^{13}C–NMR (DMSO, 50 MHz): δ 173.8, 168.9, 169.0, 166.5, 134.3, 131.8, 128.7, 127.0, 51.4, 43.2, 41.1 31.2, 27.3, 21.2, 13.4; HRMS (ESI) calcd for $C_{17}H_{24}N_3O_5$ $[M + H]^+$: 350.1710. Found: 350.1712; Anal. Calcd for $C_{17}H_{23}N_3O_5$: C, 58.44; H, 6.64; N, 12.03. Found: C, 58.24; H, 6.82; N, 11.90.

4.1.3. Cleavage of *tert*-Butyl Protecting Group

A solution of the *tert*-butyl ester derivative (1 mmol) in 50% TFA/CH_2Cl_2 (0.5 M) was stirred for 2 h at room temperature. After the completion of the reaction, the organic solvent was evaporated under reduced pressure and the residue was purified by recrystallization.

(R)-9-Butyl-1,4,7,10-tetraoxo-1-phenyl-2,5,8,11-tetraazatridecan-13-oic acid (**16a**). Yield 87%; White solid; mp 195–206 °C; $[\alpha]_D^{20}$ + 20.0 (*c* 1.00, CH_3OH); ^{1}H–NMR (CD_3OD, 200 MHz): δ 7.91–7.77 (m, 2H, arom), 7.59–7.35 (m, 3H, arom), 4.45–4.32 (m, 1H, NHC*H*), 4.26 (s, 2H, NHCH_2), 4.05 (s, 2H, NHCH_2), 3.90 (s, 2H, NHCH_2), 1.97–1.57 (m, 2H, CH_2), 1.41–1.16 (m, 4H, CH_2), 0.86 (t, *J* = 6.6 Hz, 3H, CH_3); ^{13}C–NMR (CD_3OD, 50 MHz): δ 173.2, 171.8, 171.2, 170.2, 169.2, 133.3, 132.2, 128.7, 127.5, 53.6, 43.7, 42.9, 31.6, 28.0, 22.4, 22.3, 13.9; HRMS (ESI) calcd for $C_{19}H_{27}N_4O_6$ $[M + H]^+$: 407.1925. Found: 407.1927; Anal. Calcd for $C_{19}H_{26}N_4O_6$: C, 56.15; H, 6.45; N, 13.79. Found: C, 55.84; H, 6.62; N, 13.65.

4.2. Biology

4.2.1. Cell Culture

The methods used for the isolation, characterization and cultivation of rat renal mesangial cells have been previously described in details [29]. Confluent cells were incubated in 24-well-plates for 4 h in serum-free DMEM including 0.1 mg/mL of fatty acid-free bovine serum albumin. Subsequently, cells were preincubated for 20 min either with the vehicle or the indicated concentrations of the various inhibitors prior to stimulation with IL1β (1 nM) plus Fk (5 μM) in the presence of the inhibitors for 24 h. The total stimulation volume per well was 500 μL. Cell supernatants were taken for PGE_2 quantification.

4.2.2. Quantification of Prostaglandin E_2

A PGE_2-specific enzyme-linked immunosorbent assay (ELISA) kit (from Enzo Life Science, Lörrach, Germany) was used for the quantification of PGE_2 in the cell culture supernatants. 100 μL of the supernatants were processed according to the manufacturer's instructions.

4.2.3. Statistical Analysis

Statistical analysis of data was performed using one-way ANOVA following Bonferroni post-hoc test for multiple comparisons.

Acknowledgments: This research has been co-financed by the European Union (European Social Fund—ESF) and Greek national funds through the Operational Program "Education and Lifelong Learning" of the National Strategic Reference Framework (NSRF)—Research Funding Program: Heracleitos II. Investing in knowledge society through the European Social Fund.

Author Contributions: G.K. and A.H. conceived and designed the experiments; S.V. and O.P. performed the experiments; S.V., O.P., T.M., A.H. and G.K. contributed to the analysis of the data; S.V. and G.K. wrote the paper.

Conflicts of Interest: The authors declare no conflict of interest.

References

1. Dennis, E.A.; Norris, P.C. Eicosanoid storm in infection and inflammation. *Nat. Rev. Immunol.* **2015**, *15*, 511–523. [CrossRef] [PubMed]
2. Nakanishi, M.; Rosenberg, D.W. Multifaceted roles of PGE_2 in inflammation and cancer. *Semin. Immunopathol.* **2013**, *35*, 123–137. [CrossRef] [PubMed]
3. Sterzel, R.B.; Schulze-Lohoff, E.; Marx, M. Cytokines and mesangial cells. *Kidney Int. Suppl.* **1993**, *39*, S26–S31. [PubMed]
4. Gomez-Guerrero, C.; Hernandez-Vargas, P.; Lopez-Franco, O.; Ortiz-Munoz, G.; Egido, J. Mesangial cells and glomerular inflammation: From the pathogenesis to novel therapeutic approaches. *Curr. Drug Targets Inflamm. Allergy* **2005**, *4*, 341–351. [CrossRef] [PubMed]
5. Kokotou, M.G.; Limnios, D.; Nikolaou, A.; Psarra, A.; Kokotos, G. Inhibitors of phospholipase A_2 and their therapeutic potential: An update on patents (2012–2016). *Expert Opin. Ther. Pat.* **2017**, *27*, 217–225. [CrossRef] [PubMed]
6. Dennis, E.A.; Cao, J.; Hsu, Y.-H.; Magrioti, V.; Kokotos, G. Phospholipase A_2 enzymes: Physical structure, biological function, disease implication, chemical inhibition, and therapeutic intervention. *Chem. Rev.* **2011**, *111*, 6130–6185. [CrossRef] [PubMed]
7. Psarra, A.; Nikolaou, A.; Kokotou, M.G.; Limnios, D.; Kokotos, G. Microsomal prostaglandin E_2 synthase-1 inhibitors: A patent review. *Expert Opin. Ther. Pat.* **2017**, *27*, 1047–1059. [CrossRef] [PubMed]
8. Gronich, J.; Konieczkowski, M.; Gelb, M.H.; Nemenoff, R.A.; Sedor, J.R. Inhibition of $cPLA_2$ activation by Ginkgo biloba extract protects spinal cord neurons from glutamate excitotoxicity and oxidative stress-induced cell death. *J. Clin. Investig.* **1994**, *93*, 1224–1233. [CrossRef] [PubMed]
9. Huwiler, A.; Staudt, G.; Kramer, R.M.; Pfeilschifter, J. Cross-talk between secretory phospholipase A_2 and cytosolic phospholipase A_2 in rat renal mesangial cells. *Biochim. Biophys. Acta* **1997**, *1348*, 257–272. [CrossRef]
10. Van der Helm, H.A.; Aarsman, A.J.; Janssen, M.J.; Neys, F.W.; van den Bosch, H. Regulation of the expression of group IIA and group V secretory phospholipases A_2 in rat mesangial cells. *Biochim. Biophys. Acta* **2000**, *12*, 215–224. [CrossRef]
11. Han, W.K.; Sapirstein, A.; Hung, C.C.; Alessandrini, A.; Bonventre, J.V. Cross-talk between cytosolic phospholipase $A_2\alpha$ ($cPLA_2\alpha$) and secretory phospholipase A_2 ($sPLA_2$) in hydrogen peroxide-induced arachidonic acid release in murine mesangial cells. *J. Biol. Chem.* **2003**, *278*, 24153–24163. [CrossRef] [PubMed]
12. Beck, S.; Lambeau, G.; Scholz-Pedretti, K.; Gelb, M.H.; Janssen, M.J.W.; Edwards, S.H.; Wilton, D.C.; Pfeilschifter, J.; Kaszkin, M. Potentiation of tumor necrosis factor α-induced secreted phospholipase A_2 ($sPLA_2$)-IIA expression in mesangial cells by an autocrine loop involving $sPLA_2$ and peroxisome proliferator-activated receptor α activation. *J. Biol. Chem.* **2003**, *278*, 29799–29812. [CrossRef] [PubMed]

13. Vasilakaki, S.; Barbayianni, E.; Magrioti, V.; Pastukhov, O.; Constantinou-Kokotou, V.; Huwiler, A.; Kokotos, G. Inhibitors of secreted phospholipase A_2 suppress the release of PGE_2 in renal mesangial cells. *Bioorg. Med. Chem.* **2016**, *24*, 3029–3034. [CrossRef] [PubMed]
14. Antonopoulou, G.; Barbayianni, E.; Magrioti, V.; Cotton, N.; Stephens, D.; Constantinou-Kokotou, V.; Dennis, E.A.; Kokotos, G. Synthesis of 2-oxoamides based on sulfonamide analogues of γ-amino acids and their activity on phospholipase A_2. *Bioorg. Med. Chem.* **2008**, *16*, 10257–10269. [CrossRef] [PubMed]
15. Hansford, K.A.; Reid, R.C.; Clark, C.I.; Tyndall, J.D.A.; Whitehouse, M.W.; Guthrie, T.; McGeary, R.P.; Schafer, K.; Martin, J.L.; Fairlie, D.P. D-Tyrosine as a chiral precusor to potent inhibitors of human nonpancreatic secretory phospholipase A_2 (IIa) with antiinflammatory activity. *ChemBioChem* **2003**, *4*, 181–185. [CrossRef] [PubMed]
16. Mouchlis, V.D.; Magrioti, V.; Barbayianni, E.; Cermak, N.; Oslund, R.C.; Mavromoustakos, T.M.; Gelb, M.H.; Kokotos, G. Inhibition of secreted phospholipases A_2 by 2-oxoamides based on α-amino acids: Synthesis, in vitro evaluation and molecular docking calculations. *Bioorg. Med. Chem.* **2011**, *19*, 735–741. [CrossRef] [PubMed]
17. Vasilakaki, S.; Barbayianni, E.; Leonis, G.; Papadopoulos, M.G.; Mavromoustakos, T.; Gelb, M.H.; Kokotos, G. Development of a potent 2-oxoamide inhibitor of secreted phospholipase A_2 guided by molecular docking calculations and molecular dynamics simulations. *Bioorg. Med. Chem.* **2016**, *24*, 1683–1695. [CrossRef] [PubMed]
18. Lipinski, C.; Lombardo, F.; Dominy, B.; Feeney, P. Experimental and computational approaches to estimate solubility and permeability in drug discovery and development settings. *Adv. Drug Deliv. Rev.* **1997**, *23*, 3–26. [CrossRef]
19. Henninot, A.; Collins, J.C.; Nuss, J.M. The current state of peptide drug discovery: Back to the future? *J. Med. Chem.* **2017**. [CrossRef] [PubMed]
20. Huwiler, A.; Feuerherm, A.J.; Sakem, B.; Pastukhov, O.; Filipenko, I.; Nguyen, T.; Johansen, B. The ω3-polyunsaturated fatty acid derivatives AVX001 and AVX002 directly inhibit cytosolic phospholipase A2 and suppress PGE2 formation in mesangial cells. *Br. J. Pharmacol.* **2012**, *167*, 1691–1701. [CrossRef] [PubMed]
21. Frackenpohl, J.; Arvidsson, P.I.; Schreiber, J.V.; Seebach, D. The outstanding biological stability of β- and γ-peptides toward proteolytic enzymes: An in vitro investigation with fifteen peptidases. *ChemBioChem* **2001**, *2*, 445–455. [CrossRef]
22. *SYBYL Molecular Modeling Software Packages*, version 8.0; Tripos: St. Louis, MO, USA, 2007.
23. *Schrödinger Suite 2009 Prime*, version 2.1; Schrödinger, LLC: New York, NY, USA, 2009.
24. Pettersen, E.F.; Goddard, T.D.; Huang, C.C.; Couch, G.S.; Greenblatt, D.M.; Meng, E.C.; Ferrin, T.E. UCSF Chimera a visualization system for exploratory research and analysis. *J. Comput. Chem.* **2004**, *25*, 1605–1612. [CrossRef] [PubMed]
25. Trott, O.; Olson, A.J. AutoDock Vina: Improving the speed and accuracy of docking with a new scoring function, efficient optimization and multithreading. *J. Comput. Chem.* **2010**, *31*, 455–461. [CrossRef] [PubMed]
26. Case, D.A.; Babin, V.; Berryman, J.T.; Betz, R.M.; Cai, Q.; Cerutti, D.S.; Cheatham, T.E., III; Darden, T.A.; Duke, R.E.; Gohlke, H.; et al. *AMBER 14*; University of California: San Francisco, CA, USA, 2014.
27. Roe, D.R.; Cheatham, T.E., III. PTRAJ and CPPTRAJ: Software for processing and analysis of molecular dynamics trajectory data. *J. Chem. Theory Comput.* **2013**, *9*, 3084–3095. [CrossRef] [PubMed]
28. Kollman, P.A.; Massova, I.; Reyes, C.; Kuhn, B.; Huo, S.; Chong, L.; Lee, M.; Lee, T.; Duan, Y.; Wang, W.; et al. Calculating structures and free energies of complex molecules: Combining molecular mechanics and continuum models. *Acc. Chem. Res.* **2000**, *33*, 889–897. [CrossRef] [PubMed]
29. Huwiler, A.; van Rossum, G.; Wartmann, M.; Pfeilschifter, J. Stimulation by extracellular ATP and UTP of the stress-activated protein kinase cascade in rat renal mesangial cells. *Br. J. Pharmacol.* **1997**, *120*, 807–812. [CrossRef] [PubMed]

Sample Availability: Not available.